Electronic Supplementary Material (ESI) for Nanoscale.

Strain tuning of the Stokes shift in atomically thin semiconductors (Electronic Supplementary Information)

Iris Niehues,[a] Philipp Marauhn,[b] Thorsten Deilmann,[b] Daniel Wigger,[c]

Robert Schmidt,[a] Ashish Arora,[a] Steffen Michaelis de Vasconcellos,[a]

Michael Rohlfing[b] and Rudolf Bratschitsch*[a]

[1]*Institute of Physics and Center for Nanotechnology, University of Münster, 48149 Münster, Germany*

[2]*Institute of Solid State Theory, University of Münster, 48149 Münster, Germany*

[3]*Department of Theoretical Physics, Wrocław University of Science and Technology, 50-370 Wrocław, Poland*

Calculated absorption and differential transmission

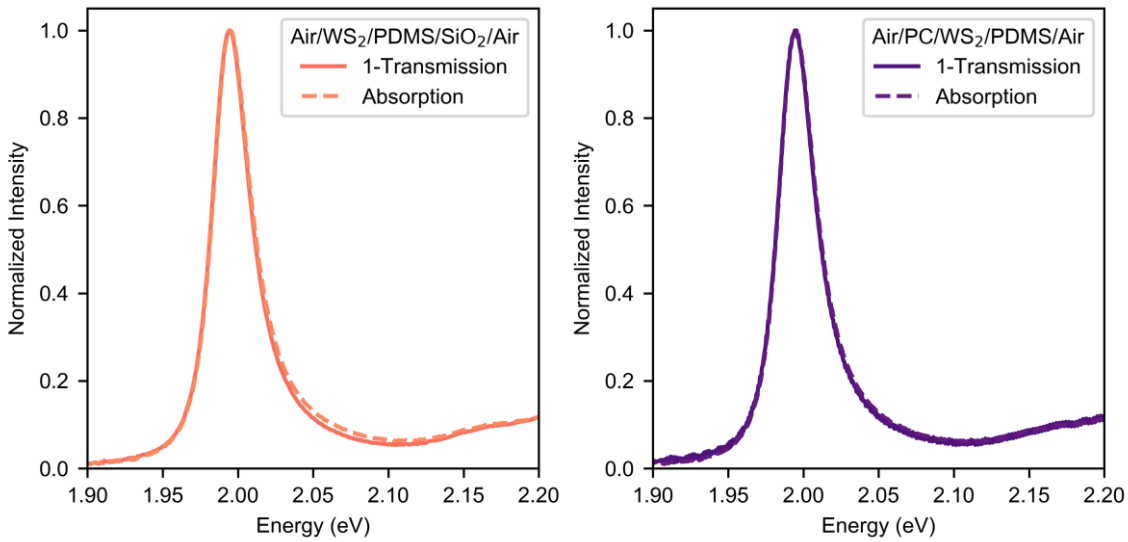

Figure S1: Transfer-matrix calculation for the two-layer stacks used in the experiment for absorption (dashed lines) and differential transmission (solid lines).

To evaluate if optical interference affects the line shape in our experiment, we compare the absorption (dashed line) with the differential transmission (1-Transmission, solid line) in a transfer-matrix calculation, taking the sample structure into account (exemplarily shown for a WS_2 monolayer in Fig. S1). The TMDC monolayers are measured as an Air/WS_2/PDMS/SiO_2/Air stack (yellow lines), the strain experiments were done on a PC substrate with Air/PDMS/WS_2/Polycarbonate/Air layering (purple lines). As shown in Fig. S1, the maximum of absorption and differential transmission are at the same energy and there is no significant difference of the line shape between the two. Therefore, one can directly extract the absorption maximum from the differential transmission measurement.

Symmetry of phonon emission in photoluminescence and differential transmission spectra

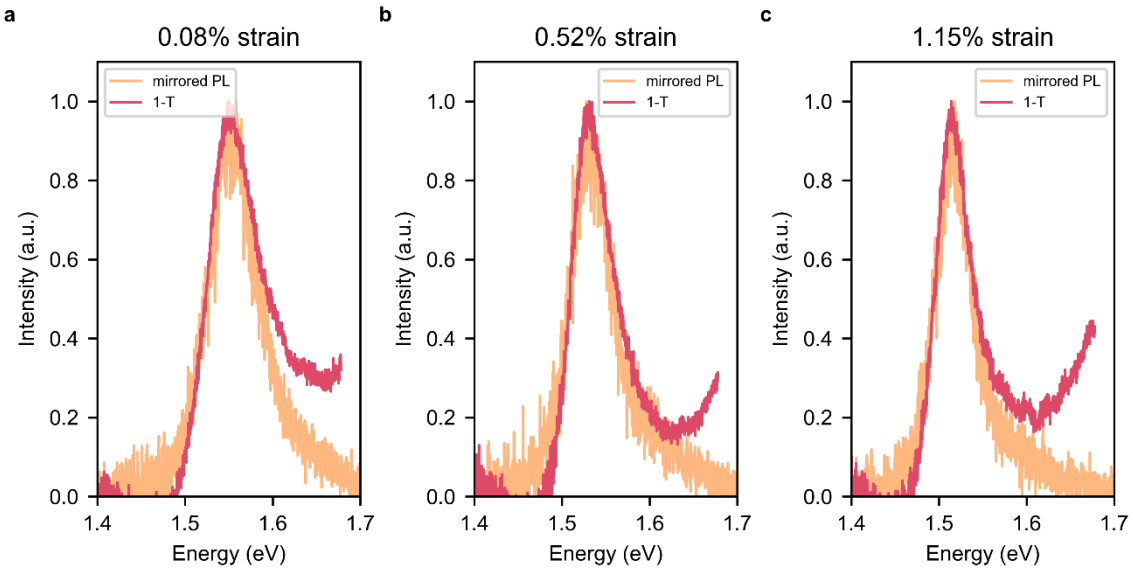

Figure S2: Comparison of the line shape of the photoluminescence (PL) (yellow) and differential transmission (pink) of the A exciton for the $MoSe_2$ bilayer due to phonon emission for different applied strain levels. The energy axis of the PL has been inverted with respect to the zero-phonon line.

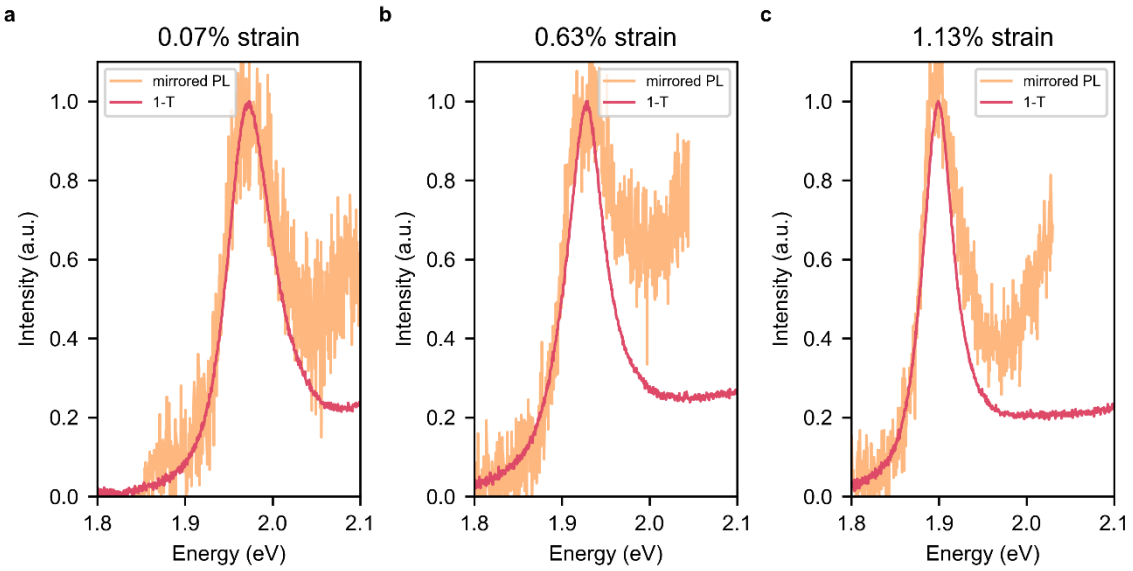

Figure S3: Comparison of the line shape of the photoluminescence (PL) (yellow) and differential transmission (pink) of the A exciton for the WS_2 bilayer due to phonon emission for different applied strain levels. The energy axis of the PL has been inverted with respect to the zero-phonon line.

Figs. S2 and S3 show the normalized PL (yellow) and differential transmission (pink) spectra of the A exciton at different strain levels for bilayer $MoSe_2$, and WS_2. To directly compare the shape of the PL with the differential transmission spectra, the energy axis of the PL has been inverted with respect to the zero-phonon line. The PL and differential transmission spectra are almost identical in a wide energy range. Small deviations on the high-energy side of the A exciton are caused by the contribution of the indirect exciton (WS_2) and the B exciton ($MoSe_2$), which overlap with the A exciton in the PL and absorption measurement, respectively.

In both absorption and photoluminescence, a possible trion signature would appear at the low-energy side of the A exciton spectrum. A comparison of the absorption spectra with the mirrored PL spectra in Figs. S2 and S3 shows that the low-energy side in both measurements is almost identical. This observation provides strong evidence that the trion does not significantly contribute to the differential transmission spectra and the line shape is governed by phononic effects at zero and increasing strain.

Temperature-dependent Stokes shift and line width in hBN-encapsulated monolayer WSe_2

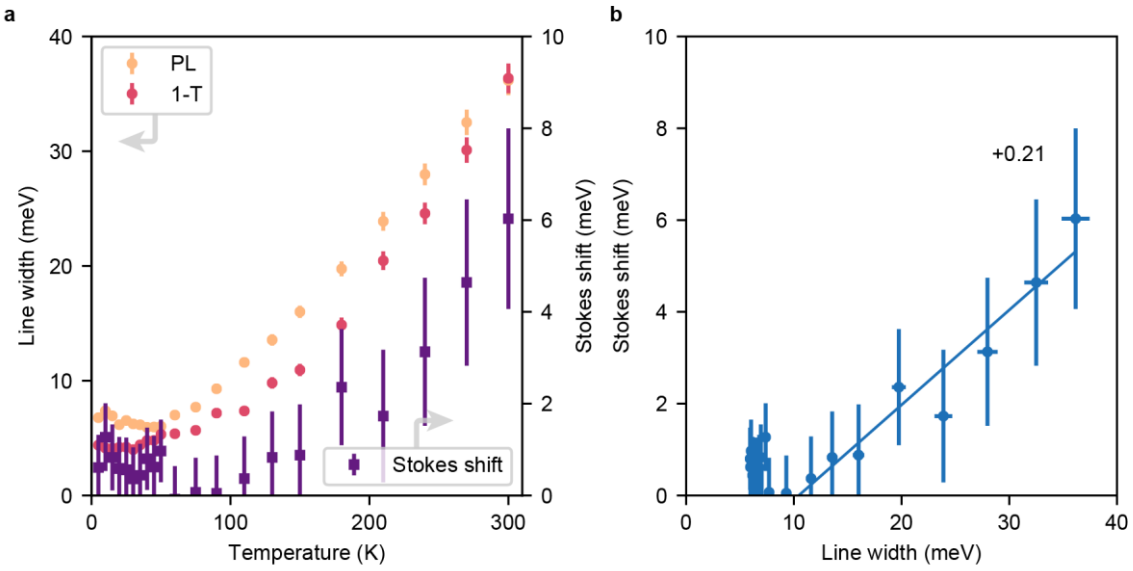

Figure S4: Temperature-dependent line width and Stokes shift in a hBN-encapsulated WSe_2 monolayer. (a) Temperature-dependent line width (FWHM) in differential transmission (pink) and PL (yellow), together with the Stokes shift in purple. Both parameters increase with increasing temperature due to enhanced phonon coupling. (b) Stokes shift vs. line width. A linear increase with a slope of (+0.21 ±0.05) is found.

Strain transfer from the substrate to the TMDC layer

FEM simulation of the strain transfer

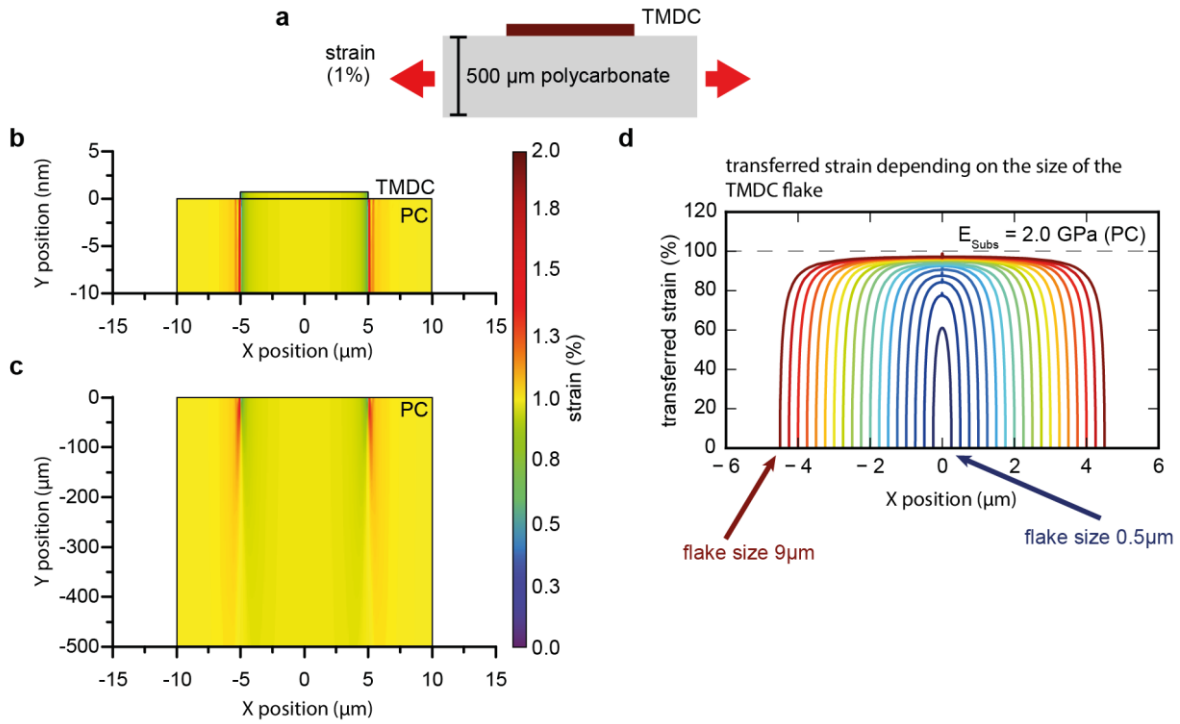

Figure S5: Finite element method (FEM) simulation of the strain transfer from an uniaxially tensile strained polycarbonate substrate to a TMDC monolayer. (a) schematic drawing of the sample. The substrate is strained by 1%. (b) Strain in the TMDC layer and PC substrate (upper 10 nm). (c) Same as (b) but plotted for the entire thickness of the PC substrate. (d) Strain distribution in the TMDC monolayer depending on the size of the TMDC flake. The transferred strain increases towards the center of the TMDC flake.

The strain profile starting from an edge towards the center of the flake can be illustrated by a finite element method (FEM) calculation (Fig. S5). The FEM calculation is performed for a monolayer with Young's modulus of (270±100) GPa[1] on top of a PC substrate of 500 µm thickness and a Young's modulus of 2.0 GPa, as it is used in the experiment (Fig. S5 (a)). In the calculation, 1% of uniaxial tensile strain is applied to the substrate. It can be seen that the strain of the substrate is not homogeneously transferred to the TMDC layer due to the strong mismatch of the Young's moduli of substrate and TMDC (Fig. S5 (b)). Interestingly, also the strain in the soft substrate is affected by the ridged TMDC itself (Fig. S5 (c)). The edges of the TMDC layer are less strained than the middle of the flake, indicated by the color gradient from green to yellow (1% strain, full transfer). Instead of a homogeneous strain in the TMDC, the strain increases from the edges towards the middle of the layer. This is shown in more detail in Fig. S5 (d), where the transferred amount of strain is plotted against the X position in the

layer and for different TMDC flake sizes (color-coded). It can be seen that the strain increases towards the center. For small flakes, e.g. the blue curve for a flake size of 0.5 µm, only a small amount of strain is transferred to the layer. In contrast, for a flake size of 8 µm (red curve) an almost complete strain transfer is reached in the middle of the TMDC flake. Already for distances of 2 µm from the edge, the layer is strained by the same amount as the substrate. The flakes used in the experiment have a minimum size of 40 µm.

Photoluminescence and Raman measurements of a WS_2 bilayer on acrylic glass substrate under uniaxial tensile strain

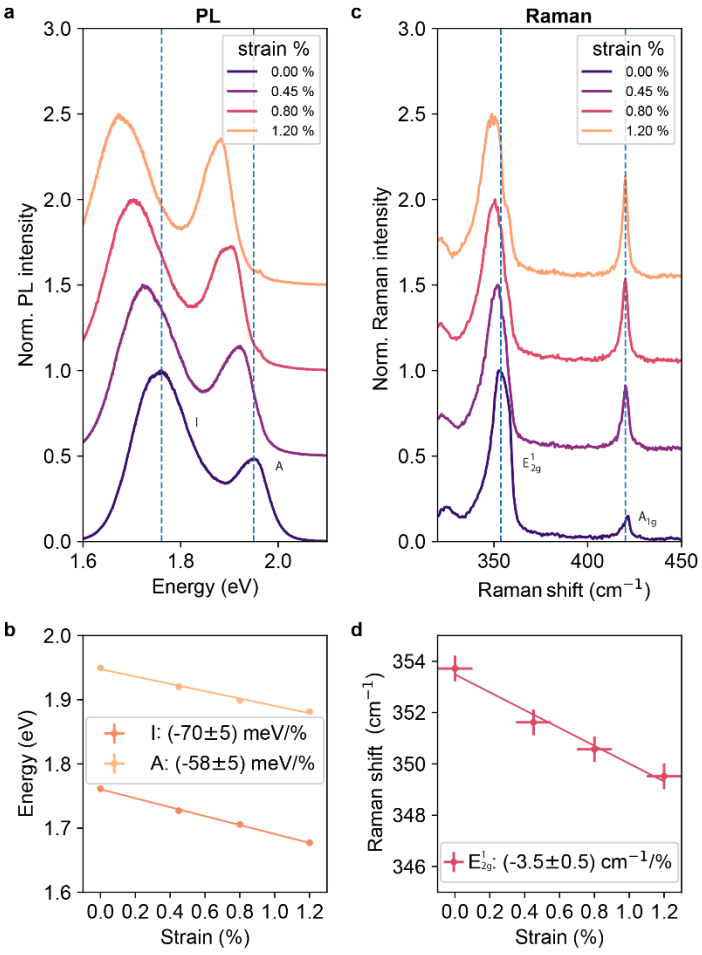

Figure S6: Photoluminescence (PL) and Raman spectra of a WS_2 bilayer on an acrylic glass substrate under uniaxial tensile strain. (a) PL spectra under strain. (b) Raman spectra under strain, measured at the same position as the corresponding PL spectra in (a). (c) Extracted gauge factors for the A and I exciton from (a). (d) Shift of the in plane E^1_{2g} mode from (c).

The Raman measurement is performed with a 532 nm laser (Coherent Verdi V-10) in a homebuilt laser scanning microscope with an objective lens (Nikon TU Plan Flour, 100x, 0.9 NA). To reduce laser sidebands a 532 nm, a laserline filter (Semrock, MaxLine LL01-523) is used. The signal is detected via a spectrometer (Andor SR 750-D1-R-SIL, grating 1800l/mm) with a sCMOS camera (Andor DU420A-BR-DD). The laser is suppressed with a 532 nm longpass (Semrock, RazorEdge Longpass, E grade 532nm) in front of the spectrometer. To avoid permanent changes of the PC substrate due to laser irradiation, we use an acrylic glass substrate (Röhm GmbH Plexiglas 0F058) with the same Young's modulus as PC for the Raman measurements.

To correlate the shift of the Raman in-plane E^1_{2g} mode with the exciton energies induced by the applied strain, we measure PL and Raman spectra at the same sample position for different amounts of strain (Fig. S6). By doing this, we can correlate the shift of the exciton energy of the PL data with the shift of the in-plane E^1_{2g} Raman mode, depending on the applied strain. Fig. S6 (a) shows the PL spectra recorded for four different strain values up to 1.2 %. The extracted gauge factors for the A and I exciton of (-58±5) meV/% and (-70±5) meV/% in Fig. S6 (b) are in excellent agreement with the ones determined for the WS_2 bilayer on the PC substrate used in the main manuscript (Fig. 5), where we found (-61±5) meV/% and (-70±5) meV/% for the A and I exciton, respectively. At the same sample position, the Raman spectra are recorded (Fig. S6 (c)). With uniaxial tensile strain, we find that the in-plane E^1_{2g} mode exhibits a softening, while the A_{1g} mode stays constant under strain, as reported earlier[2,3]. We do not observe a clear E^1_{2g} mode splitting up to 1.2 % (as observed for other TMDCs at higher tensile strain , e. g. for MoS_2 in Ref.[2]), which is in accordance with earlier measurements on a WS_2 monolayer, where a splitting was only observed at strain levels above 2 %[4], which we do not reach in our experiment. The extracted gauge factor of the E^1_{2g} mode of (-3.5+-0.5) cm^{-1}/% for our investigated WS_2 bilayer (Fig. S6 (d)) is in agreement with the measured value of -4 cm^{-1}/% for bilayer MoS_2[2] and with calculations for monolayer WS_2 yielding -3.7 cm^{-1}/%[5]. From the gauge factors of the Raman and PL measurements in Figs. S6 (b) and (d), it can be seen that the shift of the exciton energy directly corresponds to the shift of the Raman mode and therefore to the applied strain.

Furthermore, we measure PL and Raman spectra at 10 locations along the sample at a constant applied uniaxial tensile strain level of 0.9 % (Fig. S7). The PL in (a) and Raman spectra in (b) are measured at the positions marked in the PL image in (c), ordered from the bottom to the top of the bilayer (indicated by arrows). Indeed, the spectra change across the TMDC flake due to the spatially varying strain transfer from the substrate to the flake, as described in Fig. S5. The maximum shift in PL and Raman is observed at Y=54 µm (orange curve and arrow, 0.9% strain), while the minimum shift is observed at positions at the flake edges (purple arrows, black and yellow curve) and at the bottom, where the flake has cracks (darker PL emission). To investigate the shift along the WS_2 bilayer in more detail, the A exciton energy in (d) and the Raman shift of the E^1_{2g} mode in (e) is extracted from the spectra in S7(a) and (b) and plotted for the different Y positions along the flake. Note, that the extracted positions have a larger error than the given values in the main manuscript and in Fig. S6, since we

investigate areas with strain gradients leading to slightly broadened peaks due to averaging effects, which makes the determination of the maxima more challenging. Nevertheless, it becomes clear that both the A exciton energy and the Raman shift of the E^1_{2g} mode exhibit the same behavior along the flake: The shifts observed in PL and Raman increase from the edges towards the center, indicating that the strain also increases. The extracted values in PL and Raman and the determined gauge factors from Figs. S6 (b,d) are used to calculate the strain values along the flake (Fig. S7 (f)). The strain values determined from the two types of measurements agree very well.

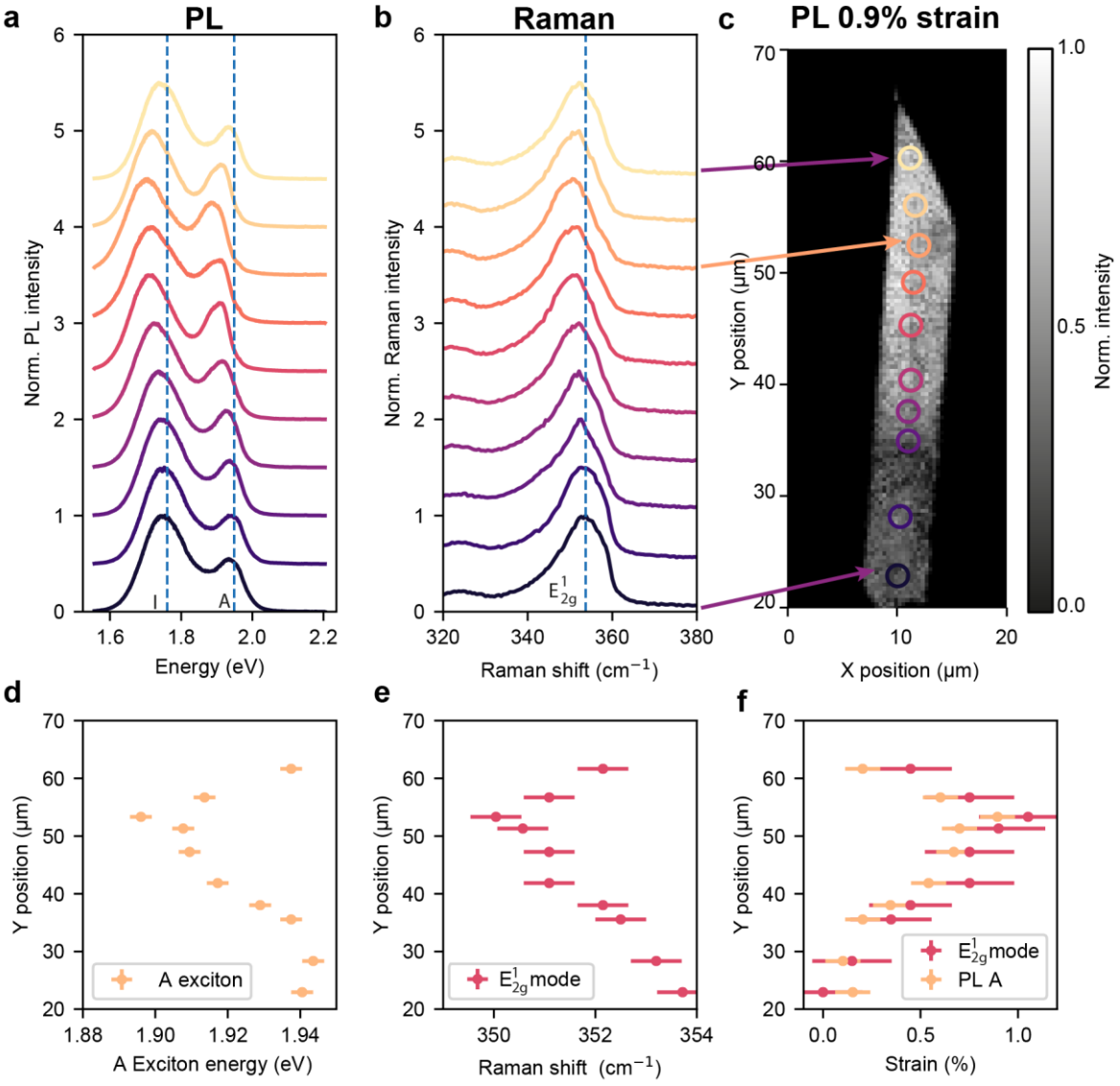

Figure S7: Photoluminescence (PL) and Raman map across a WS_2 bilayer at 0.9% applied uniaxial tensile strain. (a) PL spectra measured along the Y position of the flake shown in (c). The positions are shown from bottom to top (color-coded). (b) Same as in (a) but for Raman spectra. (c) PL map of the flake. The measurement positions are shown as color-coded circles. (d) Extracted A exciton energy along the flake from (a). (e) Extracted E^1_{2g} mode Raman shift along the flake from (b). Both quantities show the same behavior along the flake. (f) Calculated

strain values along the flake from the Raman mode shift (pink, from (e)) and from the PL shift (yellow, from (d))

$MoSe_2$ bilayer

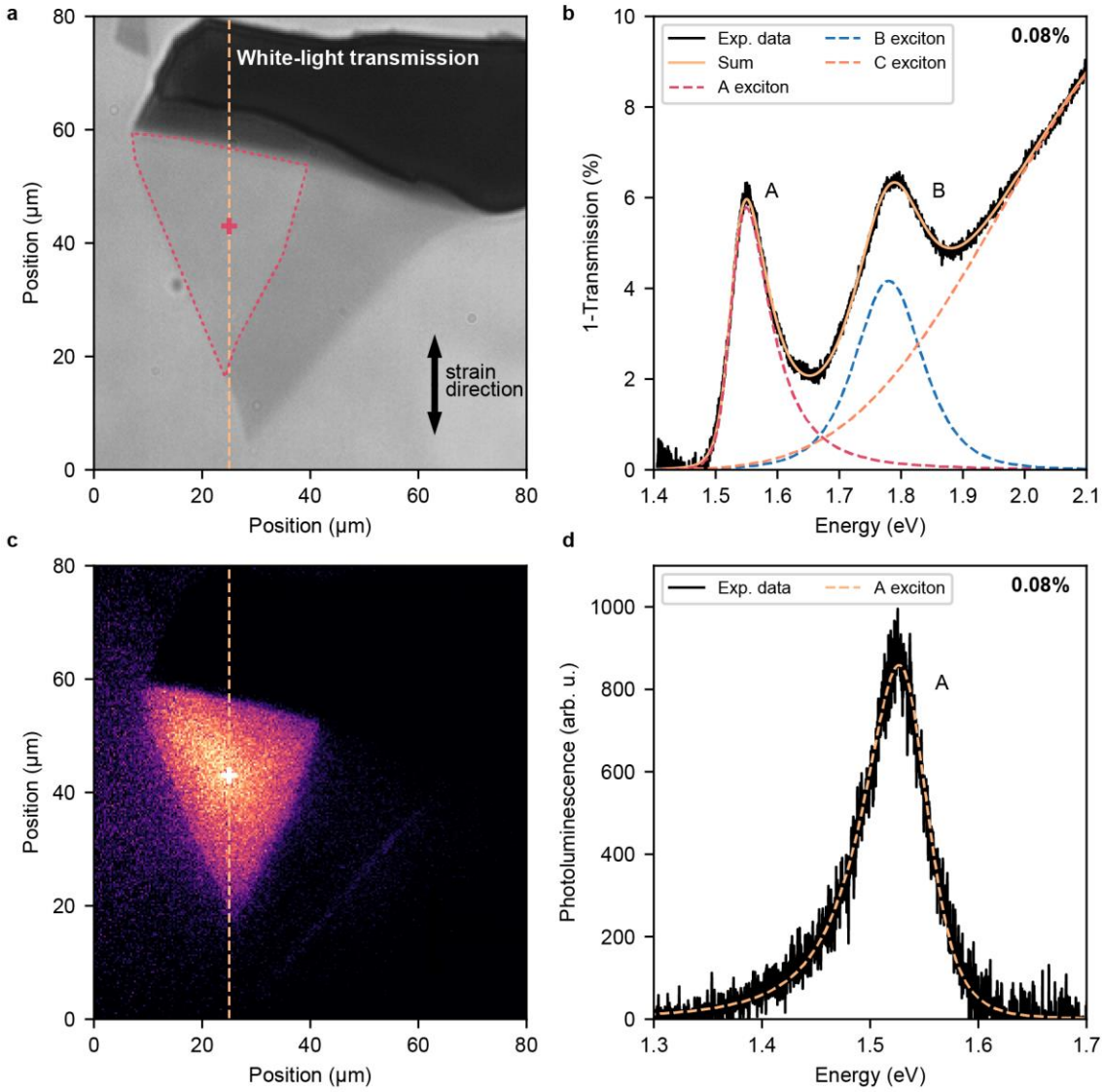

Figure S8: $MoSe_2$ Sample. (a) White-light transmission image. The strain direction is indicated by black arrow. The dashed line marks the position along which the transmission spectra are recorded. (b) Differential transmission spectra (black) from the position marked in (a) with a cross. The yellow line is the fitted curve, dashed lines represent the single resonances. (c) PL image of the bilayer similar to (a). (d) PL spectra (black) taken at the cross in (c). The dashed line represents the fitted curve (Pearson IV function).

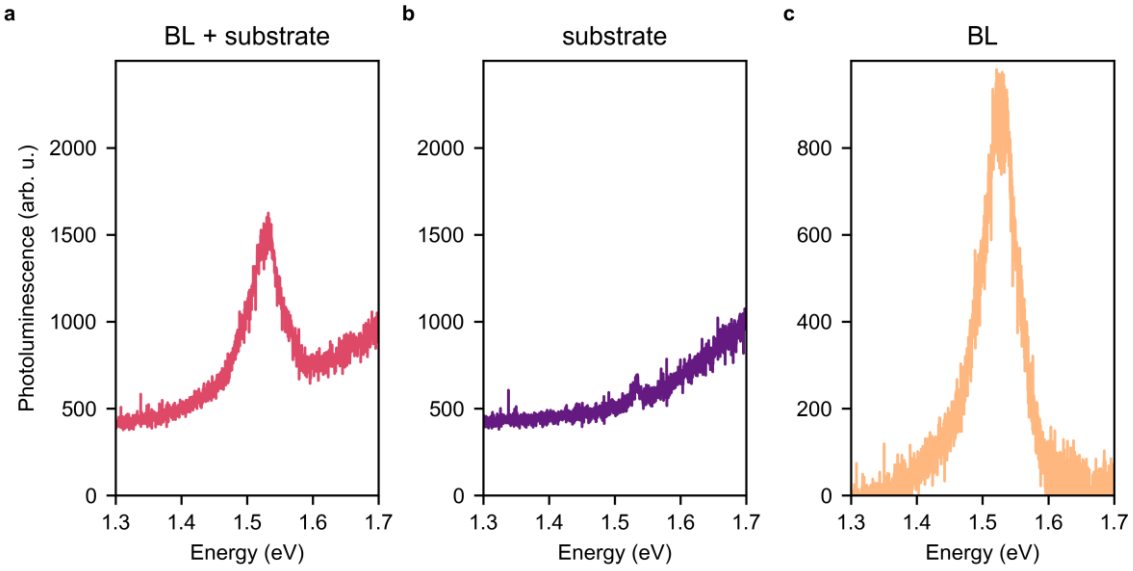

Figure S9: PL background correction of the $MoSe_2$ bilayer. (a) PL spectrum measured at the bilayer position are due to PL of the substrate and the bilayer. (b) PL spectrum of the bare substrate. (c) The difference of (a) and (b) yields the PL spectrum of the bilayer.

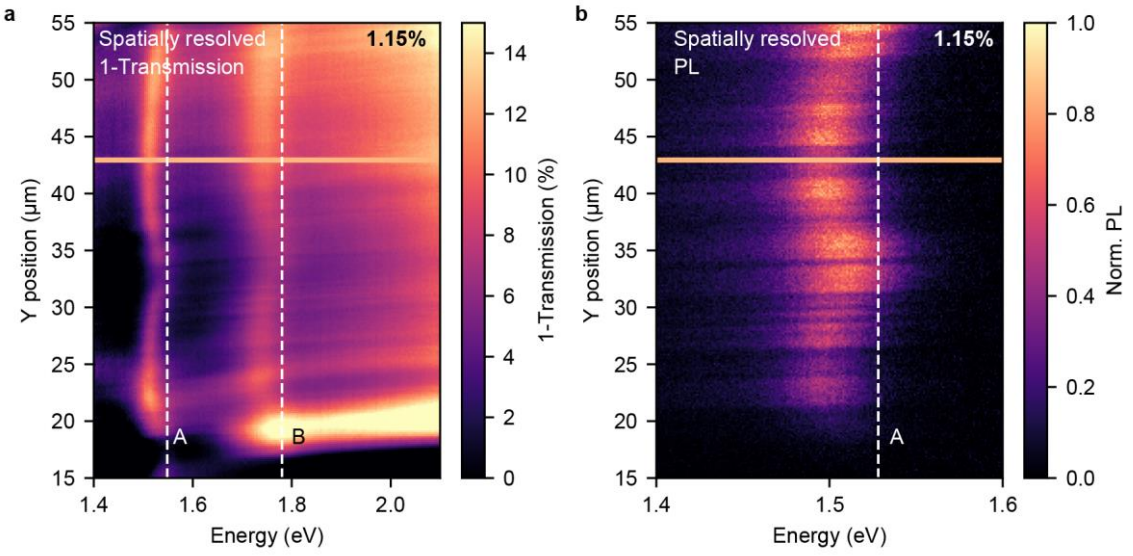

Figure S10: Exciton energy maps at maximum applied strain for $MoSe_2$. (a) Differential transmission spectra recorded along the dashed line in Fig. S5 (a). The unstrained exciton positions are marked with dashed white lines. The orange line indicates the position where the spectra during the strain measurements are extracted. A homogeneous redshift is visible in this area indicating the full strain transfer from the substrate to the bilayer. (b) Same as (a) but in PL.

Spatially resolved differential transmission and PL spectra are recorded along the vertical dashed orange line in Fig. S8 (a) for each strain value. The exciton energy maps recorded for the maximum strain value of 1.15 % are shown in Figs. S10 (a, b). The vertical dashed lines show the excitonic energy positions for the A and B excitons for the bilayer without externally

applied strain. Under strain, the exciton resonances undergo a shift to lower energies. It was shown for monolayers and bilayers that the strain transfer is spatially dependent[6] and increases from the crystal edges towards the center, leading to inhomogeneities of the strain-dependent shift in the measured spectra. Therefore, the strain transfer from the PC substrate to the $MoSe_2$ bilayer is mapped in these images. The orange line marks the position, where the spectra in the main text are analyzed. At this position, the excitons show a maximum shift, which is spatially independent over 20 µm. This observation indicates that the strain applied to the PC substrate is well transferred to the $MoSe_2$ bilayer at the investigated sample position.

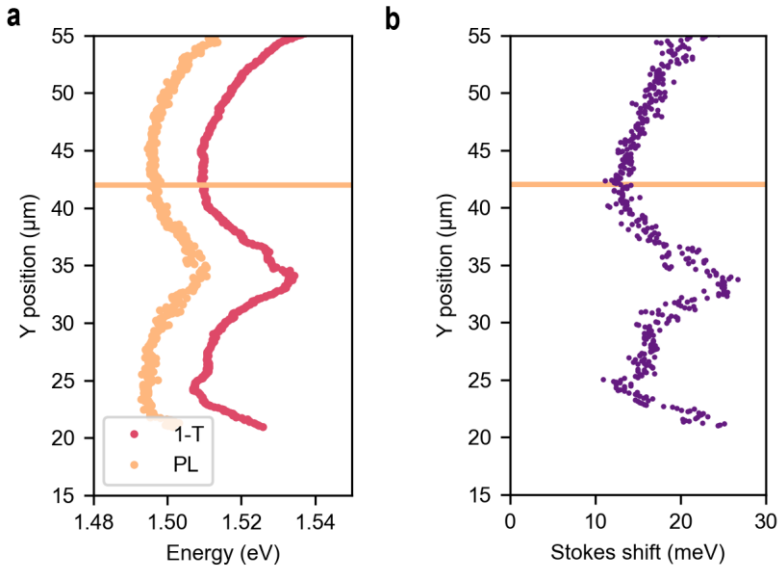

Figure S11: (a) A exciton energy map for PL (yellow) and differential transmission (pink) and (b) Stokes shift map of bilayer $MoSe_2$ calculated from the exciton energy maps. The Stokes shift is smallest in the region with highest strain, which has also the strongest energy shift of the A exciton. The map shows the inhomogeneous strain transfer to the bilayer. The analysis in the main text was carried out at a position, where exciton energy and Stokes shift are homogeneous over a few micrometers around the investigated position, indicating a full strain transfer (solid yellow line).

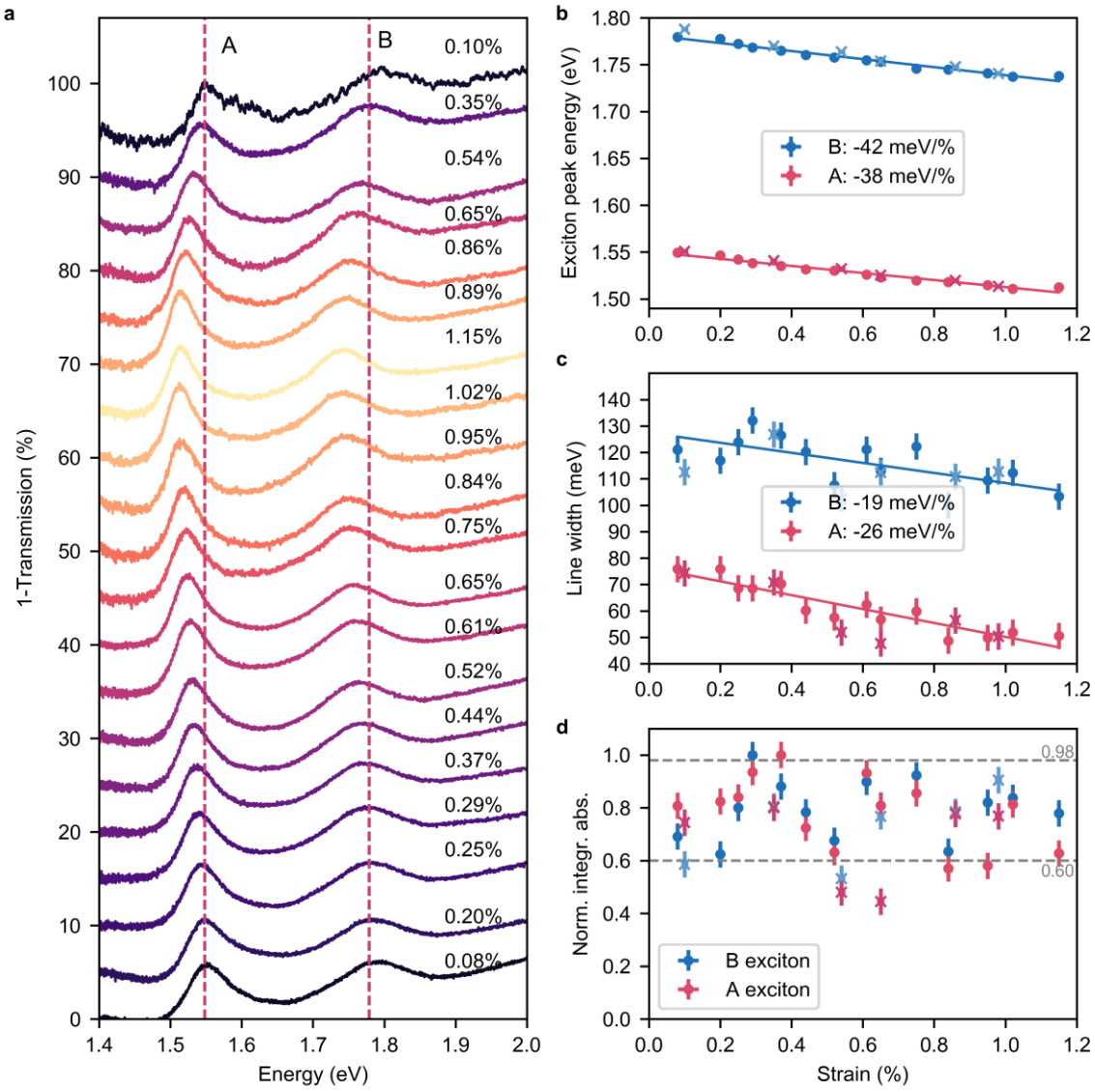

Figure S12: Differential Transmission spectra under strain of the $MoSe_2$ bilayer. (a) Spectra for increasing and decreasing levels of uniaxial strain. The strain values are color-coded from black to yellow and the spectra are drawn from bottom to top in order of data acquisition. (b) A (pink) and B (blue) exciton peak energy under strain. The gauge factors are (-39 ± 2) meV/% and (-42 ± 2) meV/%, respectively. (c) Line width under strain. The gauge factors yield (-25± 8) meV/% and (-19± 8) meV/% for A and B exciton, respectively. (d) Integrated area under strain. No trend is visible for both excitons. Increasing (decreasing) levels of strain are indicated by dots (crosses).

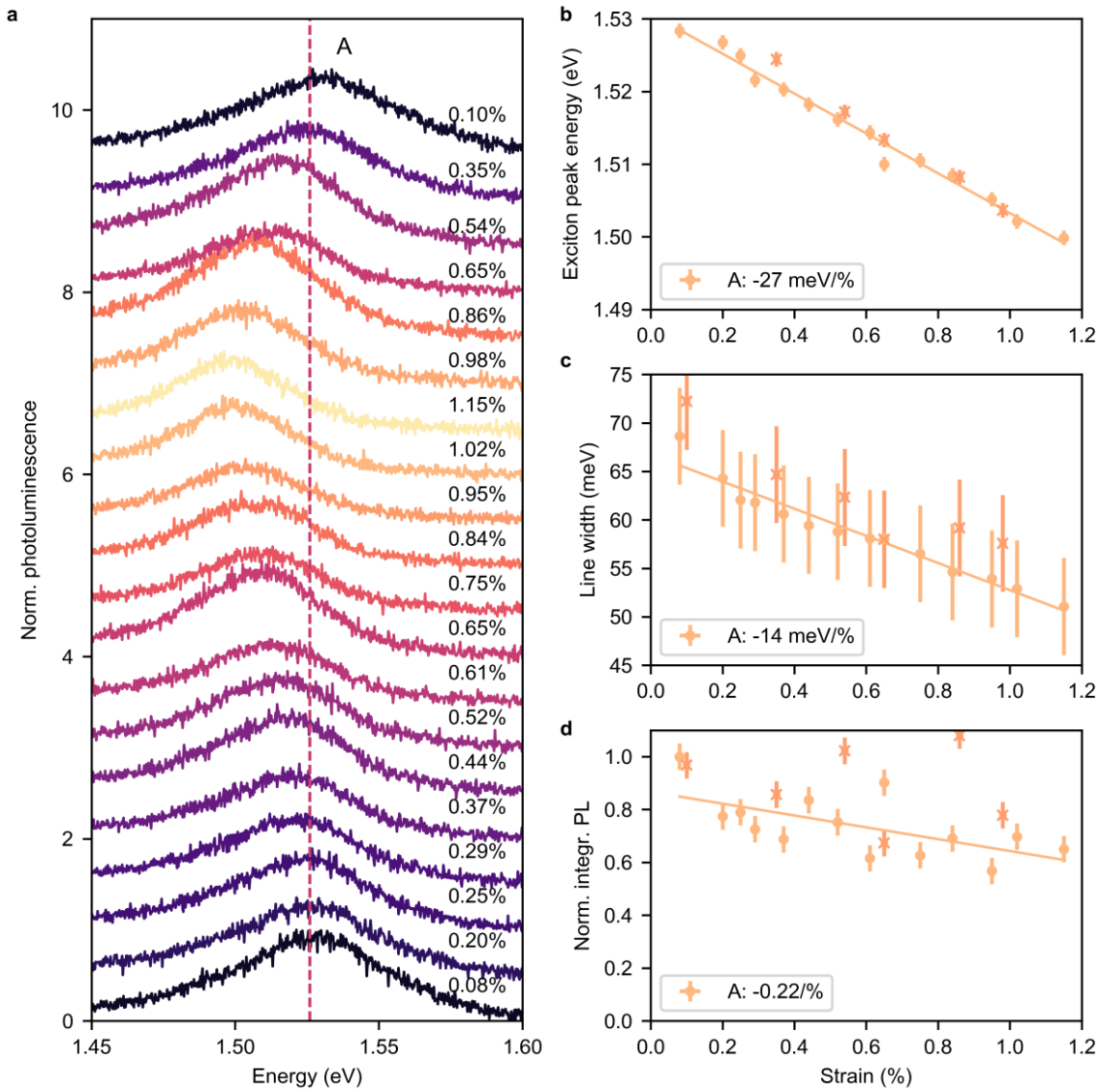

Figure S13: PL spectra under strain of the $MoSe_2$ bilayer. (a) Spectra for increasing and decreasing levels of uniaxial strain. The strain values are color-coded from black to yellow and the spectra are drawn from bottom to top in order of data acquisition. (b) A exciton peak energy under strain. The gauge factor is (-27 ± 1) meV/%. (c) Line width (FWHM) under strain. The gauge factor yields (-14± 5) meV/%. (d) Norm. integrated PL under strain. A slight decrease of -0.22/% is observed. Increasing (decreasing) levels of strain are indicated by dots (crosses).

WS_2 bilayer

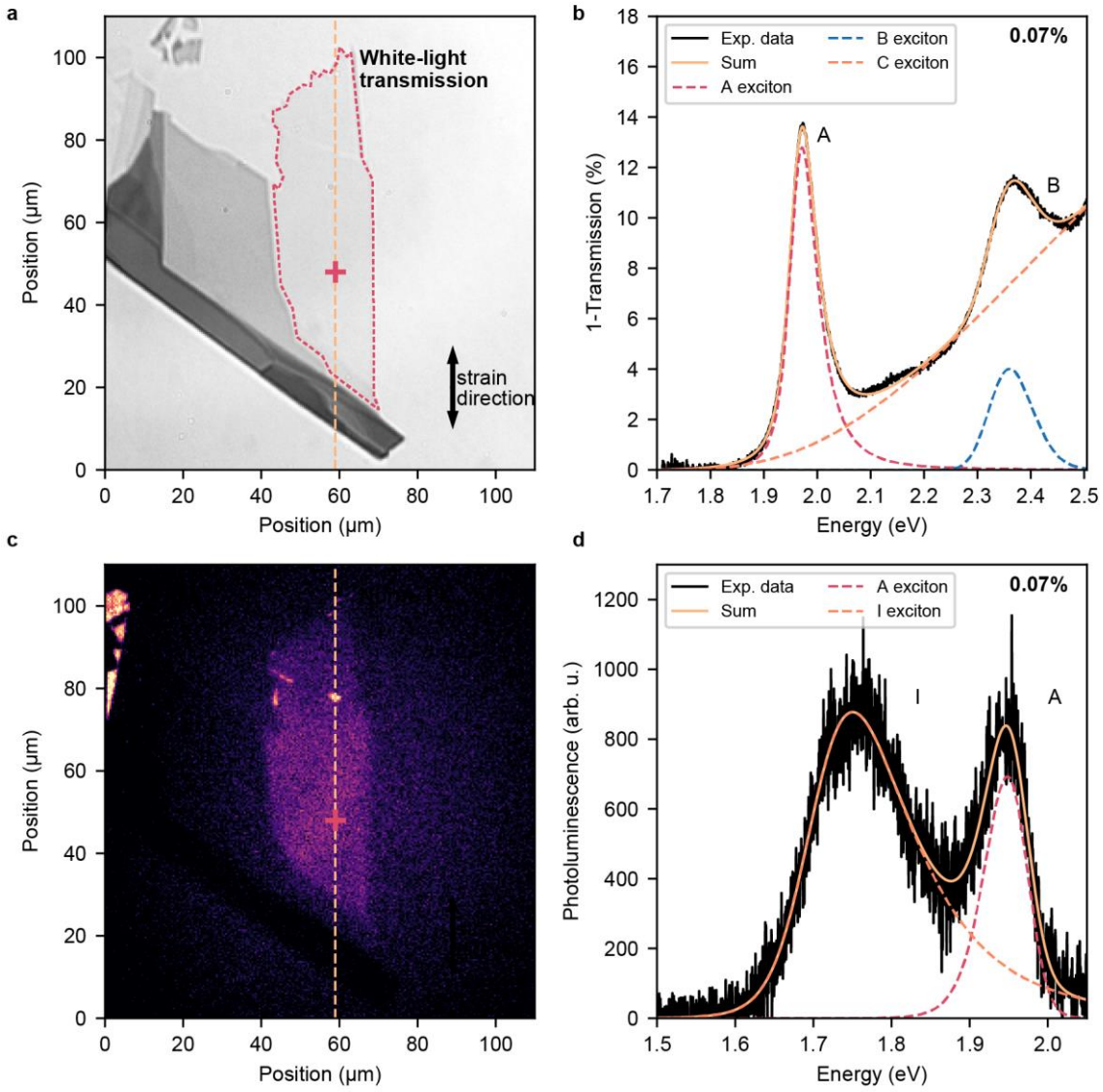

Figure S14: WS_2 sample. (a) White light transmission image. The strain direction is indicated by black arrow. The dashed line marks the position along which the transmission spectra are recorded. (b) Differential transmission spectra (black) from the position marked in (a) with a cross. The yellow line is the fitted curve, dashed lines represent the single resonances. (c) PL image of the bilayer similar to (a). (d) PL spectra (black) taken at the cross in (c). The solid line represents the fitted curve, the dashed lines the single resonances.

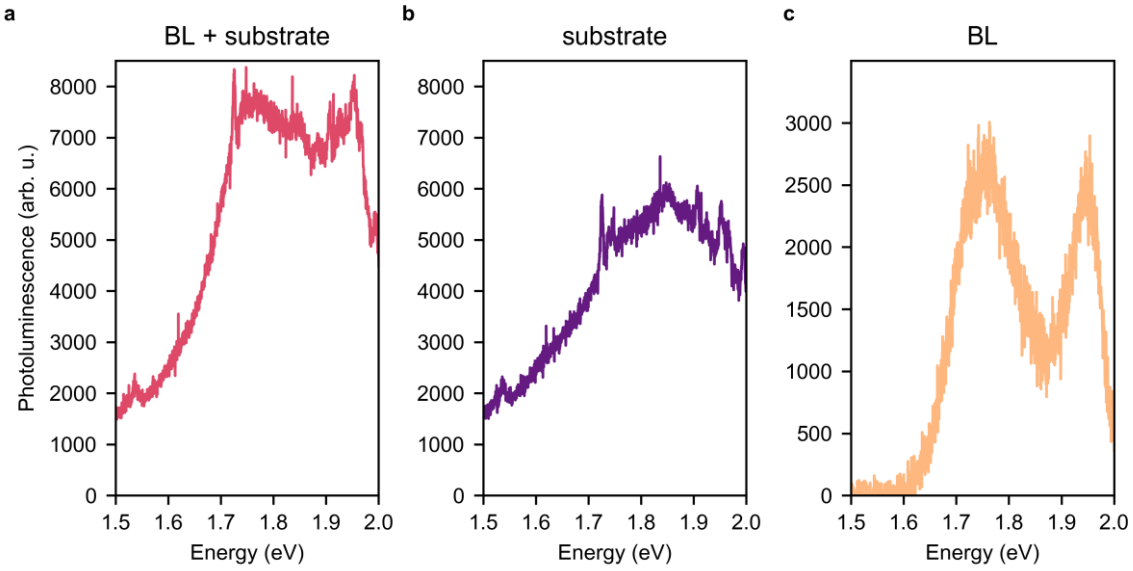

Figure S15: PL background correction of the WS_2 bilayer. (a) PL spectrum taken at the bilayer position on the substrate resembles a sum of bilayer and substrate PL. (b) PL spectrum taken on the bare substrate. (c) Difference of (a) and (b) gives the pure bilayer PL spectrum.

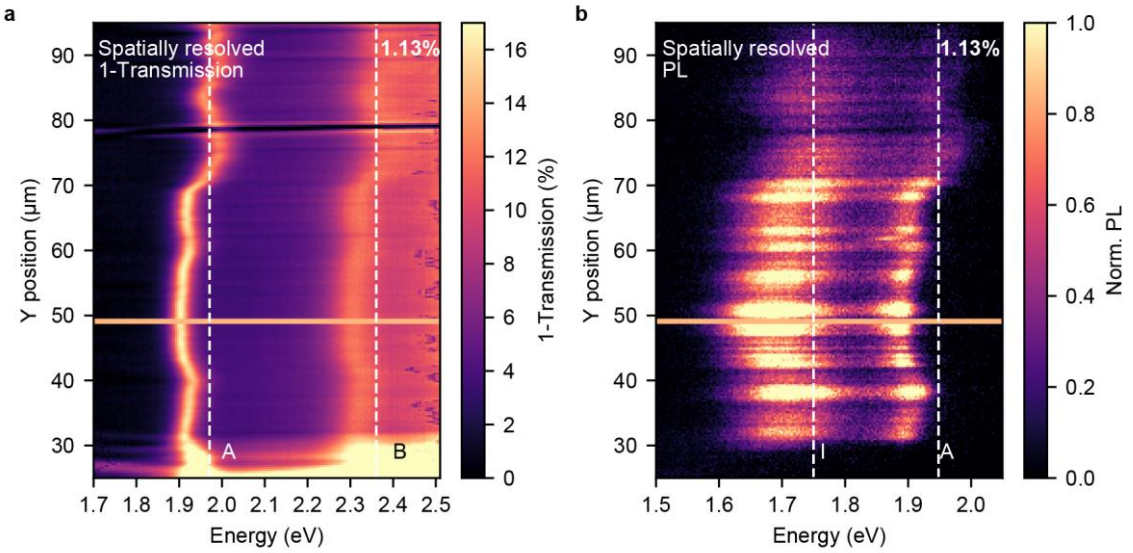

Figure S16: Exciton energy maps at maximum applied strain of the WS_2 bilayer. (a) Differential transmission spectra recorded along the dashed line in Fig. S14 (a). The unstrained exciton positions are marked with dashed white lines. The orange line indicates the position where the spectra are extracted during the strain measurements. A homogeneous redshift is visible in this area indicating the full strain transfer from the substrate to the bilayer. (b) Same as (a) but in PL.

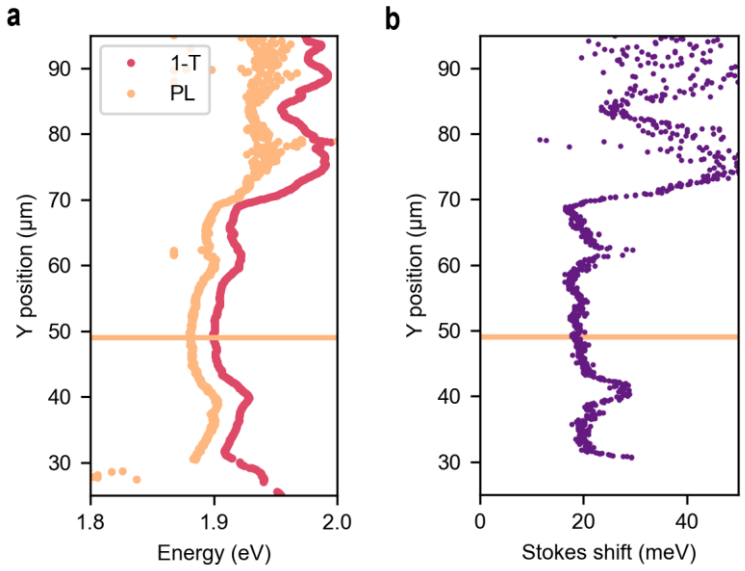

Figure S17: (a) A-exciton energy map for PL (yellow) and differential transmission (pink) and (b) Stokes shift map of bilayer WS_2 calculated from the exciton energy maps. The Stokes shift is smallest in the region with highest strain, which has also the strongest energy shift of the A exciton. The map shows the inhomogeneous strain transfer to the bilayer. The analysis in the main text was carried out at a position, where exciton energy and Stokes shift are homogeneous over a few micrometers around the investigated position, indicating a full strain transfer (solid yellow line).

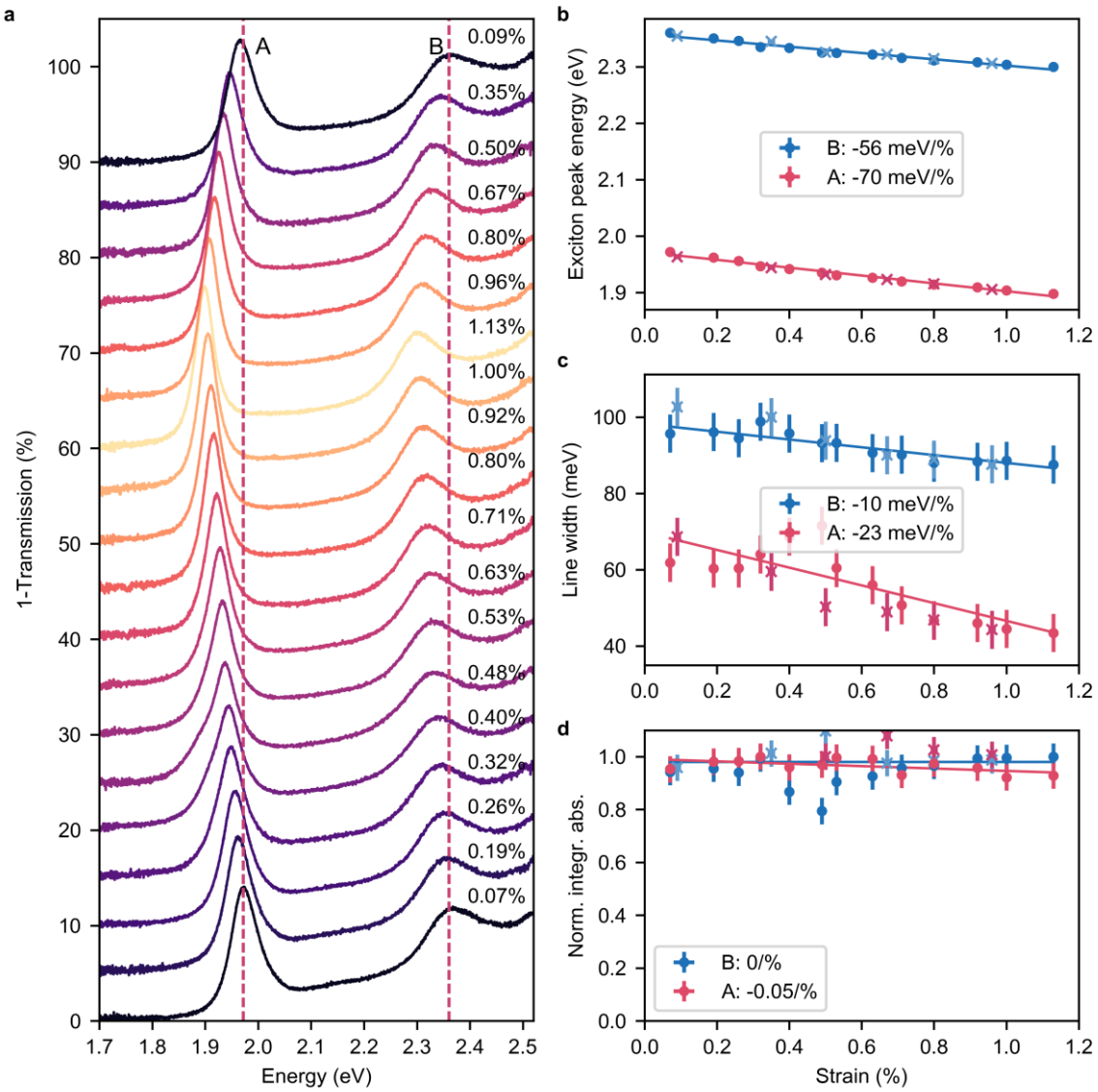

Figure S18: Differential transmission under strain of the WS_2 bilayer. (a) Spectra for increasing and decreasing levels of uniaxial strain. The strain values are color-coded from black to yellow and the spectra are drawn from bottom to top in order of data acquisition. (b) A (pink) and B (blue) exciton peak energy under strain. The gauge factors are (-70 ± 2) meV/% and (-56 ± 4) meV/%, respectively. (c) Line width (FWHM) under strain. The gauge factors yield (-23± 5) meV/% and (-10± 3) meV/% for A and B exciton. (d) Norm. integrated absorption under strain. No significant change is visible for both excitons. Increasing (decreasing) levels of strain are indicated by dots (crosses).

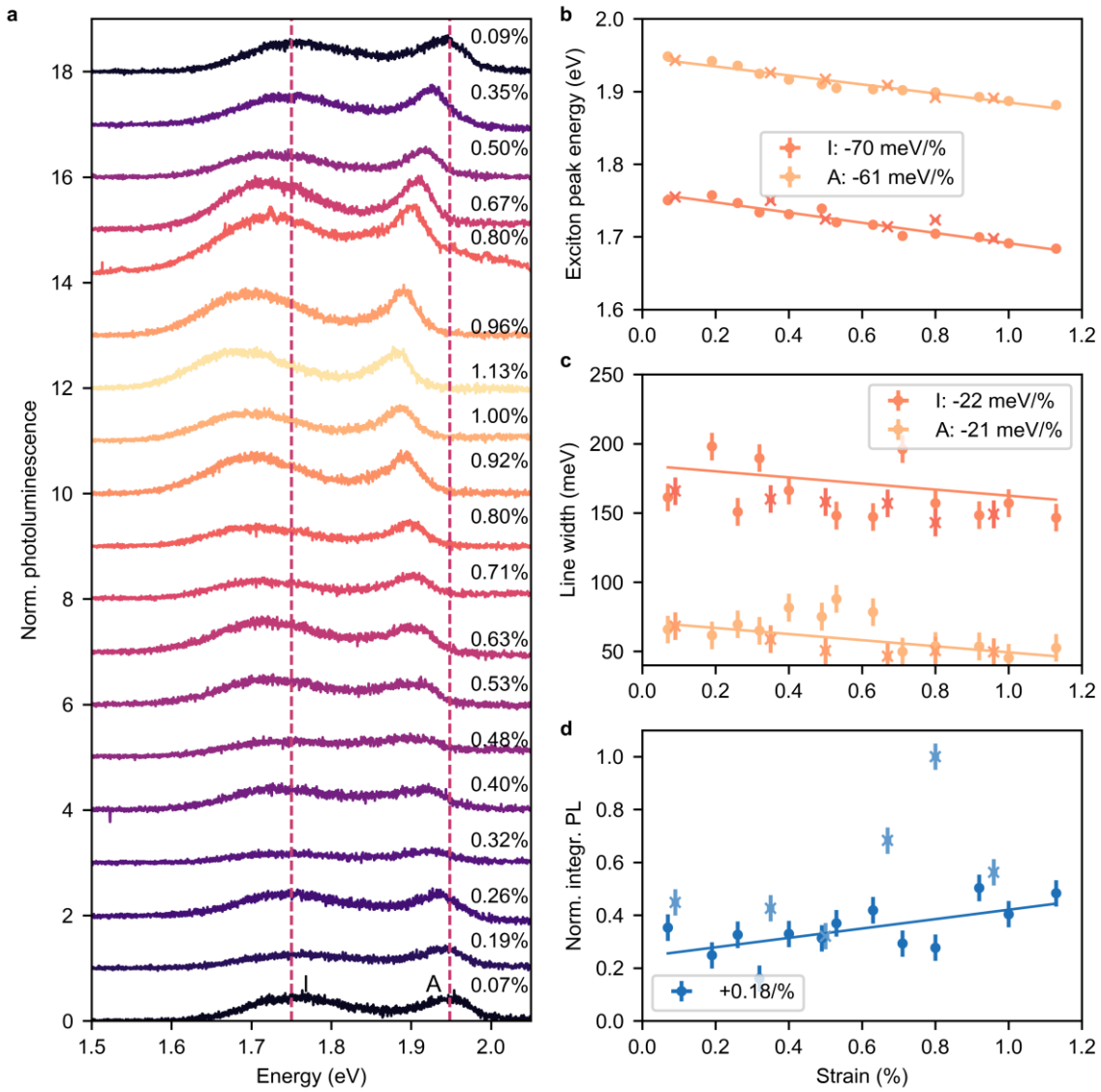

Figure S19: PL spectra under strain of the WS_2 bilayer. (a) Spectra for increasing and decreasing levels of uniaxial strain. The strain values are color-coded from black to yellow and the spectra are drawn from bottom to top in order of data acquisition. (b) A (yellow) and I (orange) exciton peak energy under strain. The gauge factors are (-61 ± 5) meV/% and (-70 ± 5) meV/%, respectively. (c) Line width (FWHM) under strain. The gauge factors yield (-21± 8) meV/% and (-22± 8) meV/% for the A and I exciton. (d) Norm. integrated PL under strain. A slight increase with (-0.18± 0.05)/% is visible for both excitons. Increasing (decreasing) levels of strain are indicated by dots (crosses).

Line shape under strain

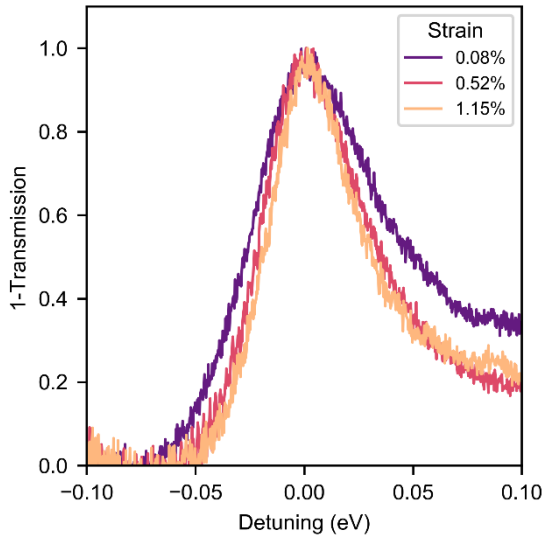

Figure S20: Line width of bilayer $MoSe_2$ in differential transmission under strain. With increasing levels of strain, the spectrum becomes narrower and more symmetric.

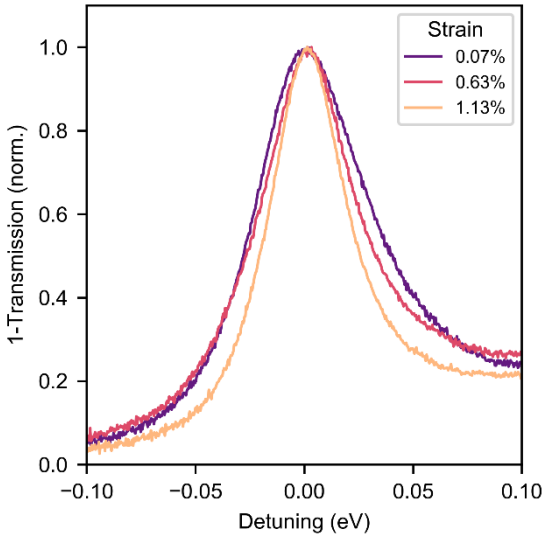

Figure S21: Line width of bilayer WS_2 in differential transmission under strain. With increasing levels of strain, the spectrum becomes narrower and more symmetric.

Quasiparticle band gaps under strain

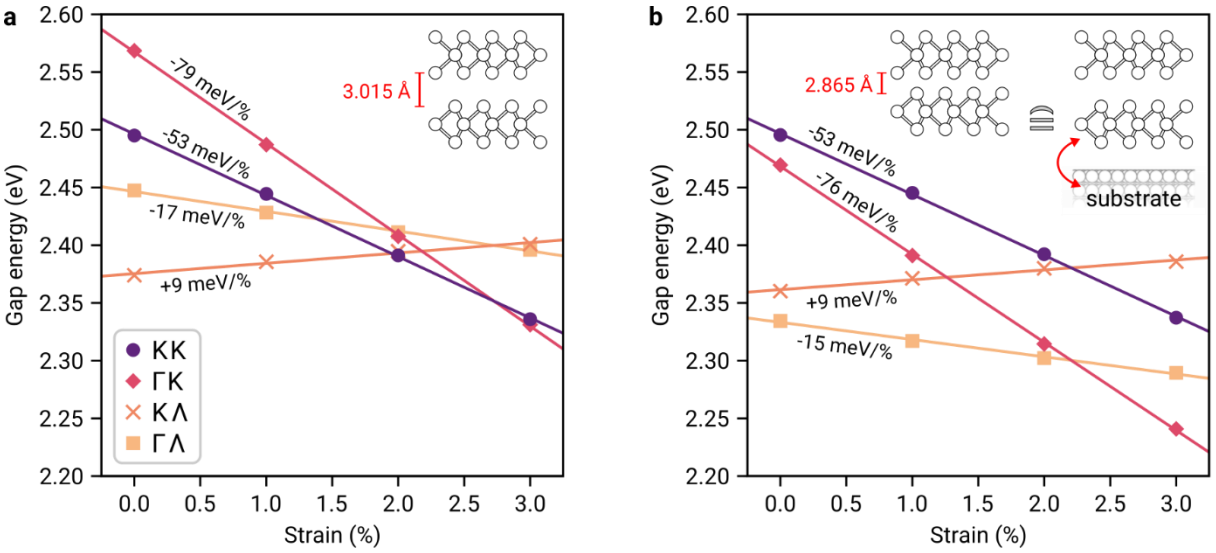

Figure S22: Quasiparticle band gaps of the WS_2 bilayer under strain. (a) Several quasiparticle gaps as a function of applied strain. Just like in Fig. 5 (f) in the main text, the interlayer distance (sulphur – sulphur) of the WS_2 bilayer is fixed at the experimentally obtained value of 3.015 Å (see Methods section). (b) To simulate the enhanced hybridization due to the substrate a smaller interlayer distance of 2.865 Å is employed. All gaps are shifted by 0.014 eV in energy to match the direct KK gap (purple) at 0% strain between (a) and (b). The gauge factors are almost the same while the energetic ordering of the band gaps is different. Most importantly, the ΓK gap (pink) is below the KK gap, which results in the band gap ordering observed in experiment (with respect to the gauge factors). The reordering of the band gaps is a result of enhanced hybridization between the two layers, shifting the relative energetic positions of the valence band valleys at Γ and K. All gaps depicted in (a) and (b) are extracted from band structure calculations within the LDA+GdW approximation.

Stokes shift vs. line width

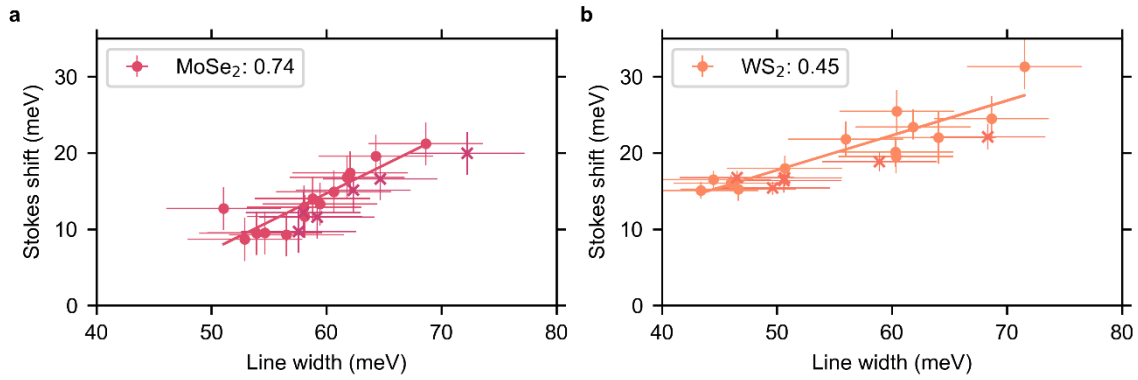

Figure S23: Stokes shift vs. line width of the A exciton in TMDC bilayers. $MoSe_2$ (a) and WS_2 (b). The extracted slopes are (0.74±0.12) for $MoSe_2$ and (0.43±0.07) for WS_2. Values from the increasing (decreasing) strain levels are shown as dots (crosses).

References

1. S. Bertolazzi, J. Brivio, and A. Kis, *ACS Nano*, 2011, **5**, 9703-9709
2. H. J. Conley, B. Wang, J. I. Ziegler, R. F. Haglund Jr., S. T. Pantelides, and K. I. Bolotin, *Nano Lett.,* 2013, **13**, 3626-3630
3. C. R. Zhu, G. Wang, B. L. Liu, X. Marie, X. F. Qiao, X. Zhang, X. X. Wu, H. Fan, P. H. Tan, T. Amand, and B. Urbaszek, *Phys. Rev. B*, 2013, **88**, 121301
4. Y. Wang, C. Cong, W. Yang, J. Shang, N. Peimyoo, Y. Chen, J. Kang, J. Wang, W. Huang and T. Yu, *Nano Res.*, 2015, **8**, 2562-2572
5. A. M. Dadgar, D. Scullion, K. Kang, D. Esposito, E. H. Yang, I. P. Herman, M. A. Pimenta, E.-J. G. Santos, and A. N. Pasupathy, *Chem. Mater.*, 2018, **30**, 5148-5155
6. R. Schmidt, I. Niehues, R. Schneider, M. Drüppel, T. Deilmann, M. Rohlfing, S. Michaelis de Vasconcellos, A. Castellanos-Gomez, and R. Bratschitsch, *2D Mater*., 2016, **3**, 021011